

---

---

# Optimization Design of Vibration Reduction Structure of Driving Sprocket Based on Niche Adaptive Genetic Algorithm

Zhangda Zhao, Wenjun Meng, Bijuan Yan, Tao Yang, Hong Ren and Yuan Yuan

Taiyuan University of science and technology, Taiyuan, 030024, China. E-mail: tyustmwj@126.com

(Received 3 December 2021; accepted 7 May 2022)

To improve the damping performance of driving sprocket of crawler construction vehicle, this paper replaces the tubular constraint “double damping layer” structure (TCDDS) with a “damping layer + stand-off-layer” structure, and the dynamics analysis of the structure is carried out under multiple working conditions. By analyzing the dynamic performance of the vibration damping structure under different working conditions, the optimal laying position of the damping layer and the stand-off-layer is discussed. Furthermore, under the condition that the total thickness of the tubular stand-off-layer sandwiched structure (TSSS) remains constant and both the stand-off-layer and damping layer do not exceed the allowable stress and strain, the energy loss ratio per unit period is taken as the optimization goal, and based on niche-adaptive genetic algorithm, the design variables (thickness of base layer, constraint layer, stand-off-layer and damping layer, material elastic modulus and loss factor of stand-off-layer and damping layer) are optimized by ANSYS and MATLAB. The optimization results show that the maximum displacement and stress of the damping layer and stand-off-layer of the structure after optimization are greatly reduced compared with those before optimization, the maximum strain increases from 15.35% to 22.55%, and the energy loss ratio increases from 0.2914 to 0.5418, which improves the vibration reduction effect of the structure. The theories and methods of this paper can provide a certain reference for the vibration damping design of heavy-duty crawler vehicles, and have a certain reference value for the application of genetic algorithm optimization in the structural design of construction vehicles.

---

## 1. INTRODUCTION

The “off-road” operating of crawler construction vehicles result in severe vibration and impact, which can easily cause the teeth of the driving sprocket to break. At the same time, the driving sprocket and crawler belt will be disengaged when meshing each other. In addition, when the impact load is transmitted to the whole body of vehicle, the various vibrations further reduce the life and working efficiency of the vehicle, and also cause some damage to the driver’s physical and mental health.<sup>1</sup>

To reduce vibration, the common method is to lay damping materials on the upper and lower layers of the original structure, such as a three-layer damping structure.<sup>2</sup> The current technology of the three-layer structure has been relatively mature, but its performance is always limited. Therefore, determining a way to improve the vibration-reducing characteristic of the damping structures has attracted the attention of many scholars. For example, Sun et al.<sup>2</sup> proposed a five-layer damping structure, which has an increased damping effect, but its manufacturing process is somewhat complicated. Yellin et al.<sup>3</sup> established a four-layer constrained damping structure, and found that this structure can increase the vibration energy dissipation. In addition, Johnson,<sup>4</sup> Zheng,<sup>5</sup> and Zhang<sup>6</sup> also further verified the research results of Yellin, and identified that adding materials with damping properties can not only increase the shear angle of the damping layer, but also increase the strain of the damping layer. However, in the practical application, it is found that if the material parameters of the

stand-off layer are not reasonably chosen, the damping characteristics of the structure may be weakened. Yan et al.<sup>7</sup> used the sub-problem approximation method to optimize the geometric parameters and loss factors of the damping structure. Zhang et al.<sup>8</sup> further discussed the influence of the laying position and elastic modulus of the stand-off layer on the vibration damping performance of TSSS. References<sup>9</sup> proposed using WFE method to effectively predict the acoustic characteristics and structural response of an infinite thin cylinder sandwich structure subjected to different internal and external excitation sources, and the numerical solution is consistent with the finite element analysis data.

In the research of the niche adaptive genetic algorithm (NAGA), it is one of the most widely utilized niching techniques. The algorithm performs selection operations by adjusting the fitness in the later generations to maintain the diversity of the population.<sup>10,11</sup> Shi<sup>12</sup> took the former two order modal loss factors and the total mass ratio of constraint damping material as the objectives, and established a multi-objective function. At the same time, the participation fitness of the genetic algorithm is used to optimize the design of the standard function, but it ignores the local minimum that may be caused by the algorithm optimization. Kumar<sup>13</sup> put forward two suggestions for the improvement of genetic algorithm with strong operability, but only put forward some instructive overview, which is not suitable for all algorithm optimization problems. In addition, the niche genetic algorithm has a limited range of adaptation and cannot be effectively effective and applica-

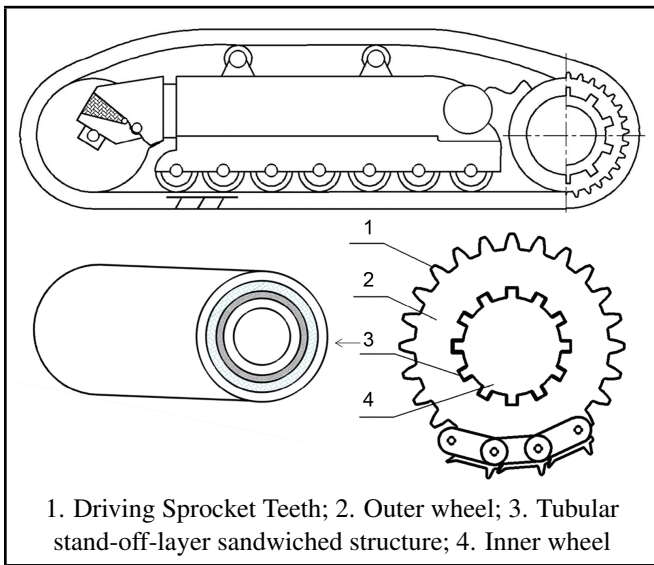


Figure 1. Driving sprocket vibration damping structure diagram.

ble to solve multi-objective and single objective optimization problems. Chen et al further verified the stability of NAGA, which can improve the ability to find better global optimal solution and speed up the convergence rate.<sup>14</sup> Bai et al found that NAGA can enhance global search capabilities through adaptive adjustments while avoiding local optima.<sup>15</sup>

At the same time, through the prior literature review, it may be found that the parameters of driving sprocket are generally optimized under a single working condition, whereas the working conditions of tracked construction vehicles are different and various, thus it is necessary to optimize the damping structure under multiple working conditions. In this paper, a certain type of 386 kW crawler bulldozer driving sprocket is used as the application object, which is shown in Fig.1. The tubular stand-off-layer sandwiched structure (TSSS) is embedded in the inner wheel of the driving sprocket. The energy loss ratio model of TSSS is established. Based on the niche technique and adaptive ideas, the improved genetic algorithm is used to optimize the structural parameters and vibration-reducing properties of the TSSS under the multi-working condition of the crawler bulldozer. Further, the dynamic response and vibration characteristics of the structure before and after optimization are compared and analyzed by using transient dynamics and modal analysis. At the same time, the vibration-reducing performance of the tubular constrained double damping layer structure (TCDDS) in the literature<sup>16</sup> under multiple working conditions is verified and analyzed. Finally, the geometric parameters and the material characteristics of damping layer and stand-off layer are calculated when the vibration damping performance of the TSSS is optimal. The theories and methods of this paper can provide a certain reference for the vibration damping design of various crawler vehicles.

## 2. MULTIPLE WORKING CONDITION ANALYSIS

In this paper, the cyclic loading test of the TCDDS was carried out on the electro-hydraulic servo program-controlled equipment according to typical working condition of crawler



Figure 2. Electro-hydraulic servo equipment.

Figure 2. Electro-hydraulic servo equipment.

bulldozers.<sup>17</sup> The test was done according to JIS k6385-2001.<sup>18</sup> The test equipment is shown in Fig. 2.

Here, the loads are divided into 8 levels according to the load amplitude ratio ( $P_i/P_{max}, i = 1, \dots, 8$ ),  $P_i$  represented the load amplitude on the tubular damping structure under various working conditions,  $i$  represents the load level, as shown in Table 1.  $P_{max}$  was the maximum load amplitude in the 8-level program load spectrum with a load size of 89.2 kN. Table 1 shows the 8-level program load spectrum, including the corresponding working conditions, the loading load value and the number of load loading cycles of each level. The probability in Table 1 represents the ratio of the number of fatigue load tests to the total number of fatigue tests of the load spectrum for the tubular damping structures under different working conditions.

When the crawler bulldozers pass over obstacles, the average of 1<sup>th</sup>, 2<sup>th</sup>, and 3<sup>th</sup> levels loads was taken as the load  $P_a$ , its loading time is 1s and it could be given as:

$$P_a = \frac{P_1 + P_2 + P_3}{3} = 83.233 \text{ (kN)}. \quad (1)$$

Similarly, taking the 4<sup>th</sup>, 5<sup>th</sup>, 6<sup>th</sup> and 7<sup>th</sup> levels loads as the load  $P_b$  under the working condition of loosening, cutting and moving conditions with a loading time of 3 s and was presented as:

$$P_b = \frac{P_4 + P_5 + P_6 + P_7}{4} = 44.6 \text{ (kN)}. \quad (2)$$

Taking the 8<sup>th</sup> level load as the load  $P_c$  under the reversing

**Table 1.** Loads at each level.

Load level	$P_i/P_{max}$	Amplitude $P_i$ /kN	Working condition	Probability	Cycles /times
1	1.0	89.2	Overstep obstacles	$1 \times 10^{-4}$	2000
2	0.95	84.7	Overstep obstacles	$4 \times 10^{-4}$	8000
3	0.85	75.8	Overstep obstacles	$2.4 \times 10^{-3}$	48000
4	0.725	64.7	Loose soil	0.016	$3.2 \times 10^5$
5	0.575	51.3	Loose soil	0.0634	$1.268 \times 10^5$
6	0.425	37.9	Loose soil, Cut soil one	0.0975	$1.95 \times 10^6$
7	0.275	24.5	Cut soil one, Cut soil two, Transport soil, Reverse	0.25	$5 \times 10^6$
8	0.125	11.2	Transport soil, Reverse	0.57	$1.14 \times 10^6$

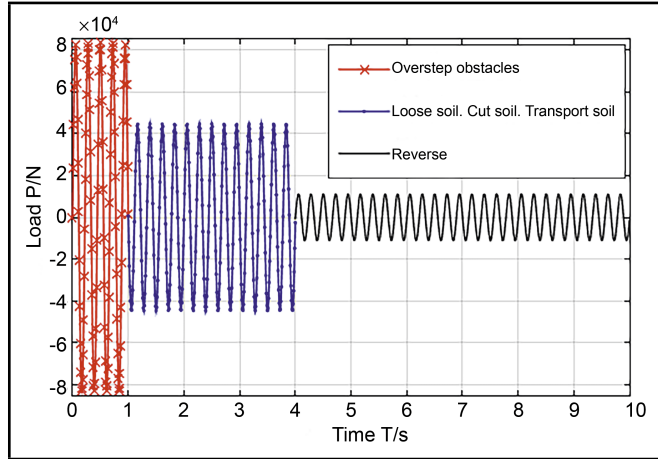


**Figure 3.** Loading under multiple working conditions.

condition with a loading time of 6s and  $P_c$  was given as

$$P_c = P_8 = 11.2 \text{ (kN)}. \tag{3}$$

Moreover, the main vibration frequency of a crawler bulldozer under typical working conditions is between 3 Hz and 8 Hz, and its first natural frequency is 4.5 Hz.<sup>7</sup> According to Eq. 1, Eq. 2, Eq. 3 and the loading duration of three typical working conditions, the loading scheme that was applied into the tubular damping structures in the ANSYS transient analysis (in Chapter 3) can be obtained, as shown in Fig. 3.

Therefore, according to Fig. 3, the loads are defined as:

$$\begin{aligned}
 F &= 83.233 * 1000 \sin\left(\frac{2\pi * \text{TIME}}{4.5}\right), 0 \leq \text{TIME} \leq 1s; \\
 F &= 44.6 * 1000 \sin\left(\frac{2\pi * \text{TIME}}{4.5}\right), 1s < \text{TIME} < 4s; \\
 F &= 11.2 * 1000 \sin\left(\frac{2\pi * \text{TIME}}{4.5}\right), 4s < \text{TIME} \leq 10s.
 \end{aligned} \tag{4}$$

### 3. OPTIMIZATION VIA NICHE-ADAPTIVE GENETIC ALGORITHM

#### 3.1. Niche-Adaptive Genetic Algorithm

Assuming that the niche radius was  $\omega_{share}$  and the distance  $d(m, n)$  between individual  $m$  and  $n$  was less than  $\omega_{share}$ , the fitness of sharing is:

$$Sh(m, n) = 1 - d(m, n)/\omega_{share}; \tag{5}$$

where  $m$  and  $n$  represented different independent variable individuals, respectively.

The fitness of individual  $m$  in the group is:

$$f_{sh,m} = 1 / \sum_{m \in pop} Sh(m, n). \tag{6}$$

In addition, the niche technology needs to randomly select a value as the initial radius of the niche. If the distance between individuals is less than the niche radius, they can be considered adjacent.

Based on the niche technique and adaptive idea,<sup>19</sup> this paper uses ANSYS and MATLAB joint optimization.<sup>20</sup> At the same time, the operator of the genetic algorithm is improved to ensure that the local optimum is jumped out and the global minimum is searched out during optimization.

Niche-Adaptive Genetic Algorithm is implemented as follows:

1. Given the counter of the number of evolutionary iterations  $r \rightarrow 0$ : randomly generate  $X$  initial individuals to form the initial population  $Q(r)$ , and obtain the dynamic fitness of all individuals in time  $f_{sh,v}(v = 1, 2, \dots, X)$ ;
2. Selection operator. For the initial population  $Q(r)$ , the proportional selection operator was used to obtain  $Q_1(r)$ . When the number of iterations  $r > S$ , the algorithm was detected whether it has fallen into the local minimum. If it has fallen into the local minimum, the fitness of the optimal solution and the individuals (assuming a total of  $Z$  individuals) close to their Hamming distance interval is as follows:  $f_{sh,w} = \lambda f_{sh,w}(w = 1, 2, \dots, Z)$ ;
3. Crossover operator. Perform uniform crossover operation on all selected individual sets  $Q_1(t)$  to obtain  $Q_2(r)$ ;
4. Mutation operator. Apply adaptive mutation operation to  $Q_2(r)$ , that is, take the mutation probability as  $q = k \cdot \sqrt{\frac{1}{d_n}}$ , where the constant parameter  $k$  was 0.1, and  $d_n$  was the Hamming distance between two random individual quantization intervals, so that  $Q_3(r)$  was obtained;
5. End condition decision. If the termination condition is satisfied, the calculation results are output and the multi condition optimization of improved genetic algorithm is completed. If the termination condition is not satisfied, update the iteration counter  $r \leftarrow r + 1$ , and then take  $Q_3(r)$  in step (4) as the population  $Q(r)$  of the next generation, and then go to step (2).

#### 3.2. Structure Optimization Parameters

The TSSS is shown in Fig. 4. The stand-off-layer and damping layer used two different damping materials, whereas

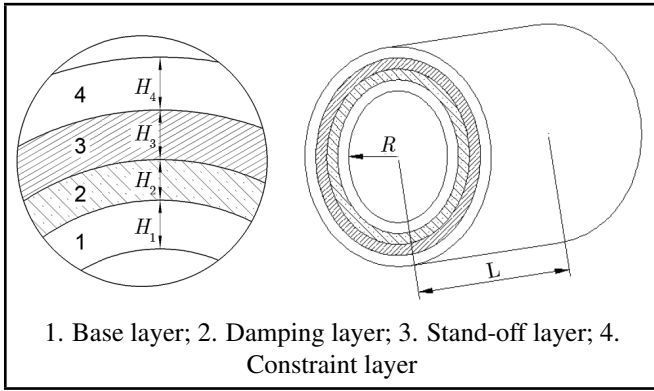


Figure 4. Schematic diagram of tubular stand-off-layer sandwiched structure.

the base and constraint layer were all made by metal materials. The thicknesses of base layer, damping layer, stand-off-layer and constraint layer of TSSS were defined as  $h = \{H_1, H_2, H_3, H_4\}$ , and the elastic modulus and material loss factor of the damping layer and the stand-off-layer were respectively  $E = \{E_q, E_2\}, \beta = \{\beta_1, \beta_2\}$ , and used these as design variables. In ANSYS, the initial values of the design variables  $H = \{0.010, 0.010, 0.010, 0.010\}m$ ,  $E = \{7.629e6, 7.629e8\}$  Pa,  $\beta = \{0.3, 0.3\}$ ,  $R=0.050$  m,  $l=0.150$  m, the structural parameters are shown in the Table 2.<sup>21</sup>

When establishing the finite element model of the TSSS, solid185 element is selected to simulate the base and constraint layer, and solid186 element is selected to replace the damping layer and stand-off layer.<sup>22</sup> At the same time, the structure is divided into  $N$  elements, which means that the number of elements of the TSSS is also  $N$ , where the numbers of elements of the base layer, constrained layer, damping layer and stand-off-layer in the structure are  $m, n, p, q$ , respectively.

### 3.3. Optimal Design

In this paper, the energy loss ratio was regarded as the optimization objection. Based on the deformation energy method,<sup>23,24</sup> the energy loss ratio  $\eta$  of the TSSS of the driving sprocket can be written as follows:

$$\eta = \frac{\sum_{i=1}^N \beta_i \Delta U_i}{\sum_{i=1}^N U_i} \quad (7)$$

In Eq. 7,  $\beta_i$  is the material loss factor;  $U_i$  was the strain energy of the  $i$ -th element;  $\Delta U_i$  was the elastic energy of the  $i$ -th unit;  $\beta_i \Delta U_i$  was the energy consumption of the  $i$ -th unit.

The elastic energy of all directions can be expressed by the stress-strain constitutive equation.<sup>25</sup> thus, the expression of  $U_i$  is:

$$\begin{aligned} U_{xx}^i &= \frac{1}{2} \int_{v_i} \sigma_{xx} \epsilon_{xx} dV_i, & U_{\theta\theta}^i &= \frac{1}{2} \int_{v_i} \sigma_{\theta\theta} \epsilon_{\theta\theta} dV_i; \\ U_{zz}^i &= \frac{1}{2} \int_{v_i} \sigma_{zz} \epsilon_{zz} dV_i, & U_{x\theta}^i &= \frac{1}{2} \int_{v_i} \tau_{x\theta} \gamma_{x\theta} dV_i; \\ U_{\theta z}^i &= \frac{1}{2} \int_{v_i} \tau_{\theta z} \gamma_{\theta z} dV_i, & U_{xz}^i &= \frac{1}{2} \int_{v_i} \tau_{xz} \gamma_{xz} dV_i; \\ U^i &= U_{xx}^i + U_{\theta\theta}^i + U_{zz}^i + U_{x\theta}^i + U_{\theta z}^i + U_{xz}^i; \end{aligned} \quad (8)$$

where  $U_{xx}^i, U_{\theta\theta}^i$ , and  $U_{zz}^i$  were the strain energy of the  $i$ -th element due to the combined bending and stretching in the  $x$ ,

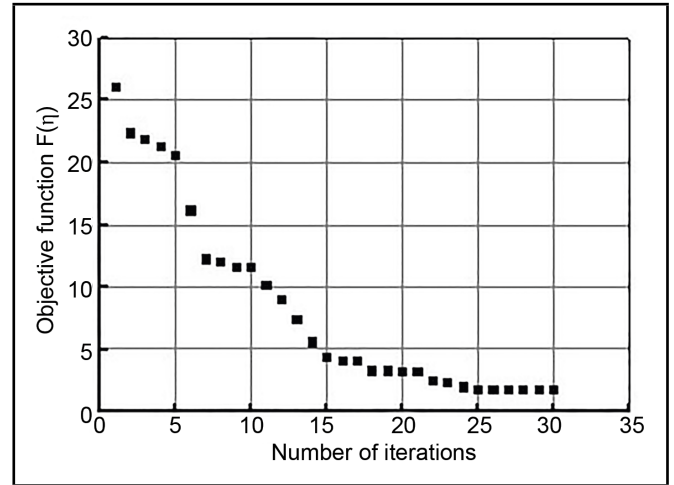


Figure 5. Improved genetic algorithm optimization iteration.

$\theta$  and  $z$  directions, respectively;  $U_{x\theta}^i, U_{xz}^i, U_{\theta z}^i$  were the strain energy of the  $i$ -th element due to the transverse shear strain;  $U^i$  is the total elastic deformation energy of the  $i$ -th element;  $V_i$  is the volume of the  $i$ -th element.

The derivation process of strain energy of each layer is shown in the appendix.

From the above Eq. 7 and Eq. 8, the energy consumption of the damping structure can be calculated, and the energy loss ratio can be obtained by Eq. 9 and Eq. 10. Where,  $D_x$  represented the energy dissipation of  $x$  in the damping structure;  $D_t$  was the total strain energy of the damping structure;  $\beta_x$  represented the material loss factor of  $x$  in the damping structure, where  $x = b, c, s, v$  (base layer, constrained layer, stand-off-layer, viscoelastic damping layer).

In this paper, the base layer and the constrained layer were regarded as incompressible, so the strain in each direction of the two layers can be ignored, and the Eq. 10 is simplified as:

$$\eta = \frac{D_s + D_v}{D_t} = \frac{\sum_{i=1}^p \beta_s \Delta U_{si} + \sum_{i=1}^q \beta_v \Delta U_{vi}}{\sum_{i=1}^{m+n+p+q} U_i} \quad (11)$$

Under the conditions that the allowable stress and strain of the stand-off-layer and the damping layer and the total thickness of the TSSS remained unchanged, the objective of the optimal design of the structure was to maximize its structural energy loss ratio. Also, the accuracy in the solution of objective function was related with iterative convergence rate, thus, the objective function was converted to the minimum value of structural energy loss ratio reciprocal. Here the energy loss ratio maximization should ensure that the stiffness and strength of structure were within the safe allowable range, is related with stiffness and strength of structure, and the minimization of the objective function was subjected to design constraints, such as maximum stress and strain ( $G_{max}, \rho_{max}$ ) of the stand-off-layer and the damping layer. Hence, the optimal configu-

**Table 2.** Parameters of the tubular stand-off-layer sandwiched structure.

	Elastic Modulus /Pa	Poisson's ratio	Density kg/m <sup>3</sup>	Thickness /m	Loss factor
Damping layer	7.629e6	0.499	1200	0.010	0.3
stand-off-layer	7.629e8	0.499	1130	0.010	0.3
Constraint layer	2.09e11	0.300	7800	0.010	0
Based layer	2.09e11	0.300	7800	0.010	0

$$\eta = \frac{D_b + D_c + D_s + D_v}{D_t}; \tag{9}$$

$$\eta = \frac{\sum_{i=1}^m \beta_b \Delta U_{bi} + \sum_{i=1}^n \beta_c \Delta U_{ci} + \sum_{i=1}^p \beta_s \Delta U_{si} + \sum_{i=1}^q \beta_v \Delta U_{vi}}{\sum_{i=1}^{m+n+p+q} U_i} \tag{10}$$

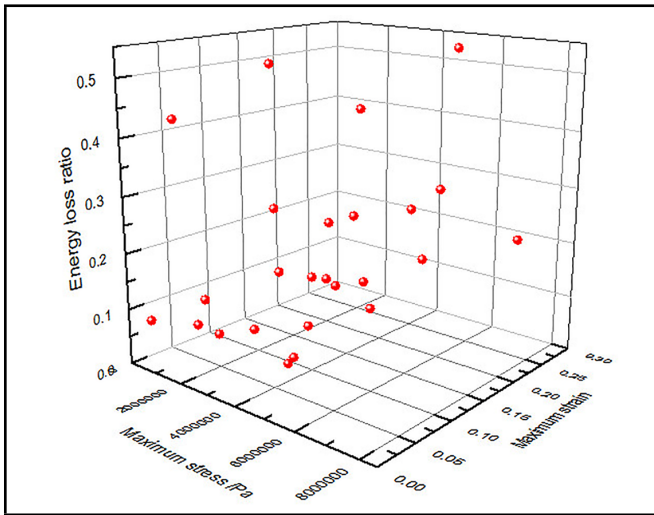


**Figure 6.** Iterative results under constraint conditions.

ration of the TSSS can be summarized as:

$$\begin{aligned} \min F &= \frac{1}{C}, \quad C = \eta; \\ 0.005\text{m} &\leq H_x \leq 0.015\text{m}, \quad \sum_{x=1}^4 H_x = 0.040\text{m}, \\ x &= \{1 \ 2 \ 3 \ 4\}; \\ 2 \times 10^5\text{Pa} &\leq E_1 < \times 10^9\text{Pa}, \\ 2 \times 10^5\text{Pa} &< E_2 \leq 2 \times 10^9\text{Pa}, \quad E_1 < E_2; \\ 0 \leq \beta_1 &\leq 0.5, \quad 0 \leq \beta_2 \leq 0.5; \\ G_{max} &\leq 8.3 \times 10^6\text{Pa}, \quad \sigma_{max} \leq 0.3; \end{aligned} \tag{12}$$

where  $H_x$  was the thickness value of each layer of the tubular stand-off-layer sandwiched structure.  $x$  represents the layer number of each layer of the TSSS, and  $X = 1, 2, 3, 4$  represents the base layer, damping layer, transition layer and constraint layer respectively.

### 3.4. Optimal Results

The iterative curve of the objective function is shown in Fig. 5. The objective function evolved for about 25 generations, and the total time consumption is about 13h. Moreover, all the iterative results conform to the allowable stress and strain ( $G_{max} \leq 8.3 \times 10^6\text{Pa}, \sigma_{max} \leq 0.3$ ). As shown in Figure 6, the optimal solution of the objective function is  $F(\eta) = 1.8457$ , the energy loss ratio  $\eta$  is 0.5418,  $H = \{0.010518607, 0.011145459, 0.0068058577, 0.0115300763\}$

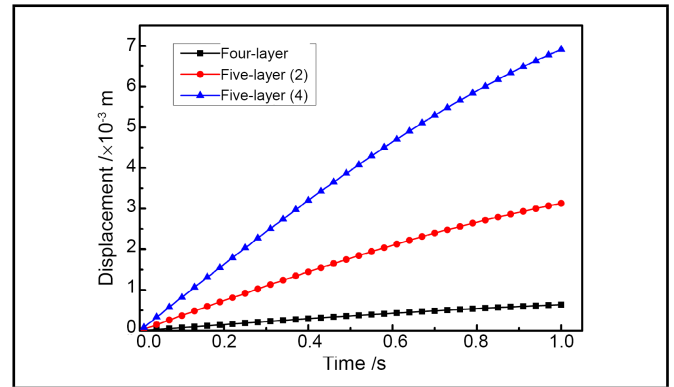


**Figure 7.** Vibration response of damping layer of two kinds of tubular damping structures.

$m, E = \{8.6234142 \times 10^6, 2.0001500 \times 10^8\}$  Pa,  $\beta = \{0.49, 0.35\}$ .

Compared with the above results, the thickness of base layer, damping layer and constraint layer of the optimized tubular stand-off-layer sandwiched structure is slightly increased compared with those before optimization, while the thickness of stand-off-layer is reduced by 0.0031941423 m, accounting for 31.941% of that before optimization; The results show that the elastic modulus of the damping layer is about 2 orders of magnitude smaller than that of the stand-off-layer, and the difference between the elastic modulus of the damping layer and that of the base/constraint layer is about 5 orders of magnitude. In addition, the energy loss ratio of the structure increases when the stand-off-layer (the elastic modulus of the material is between the constraint layer and the damping layer) is laid between the damper layer and the constraint layer, and the vibration reduction performance is the best.

## 4. DISCUSSION OF OPTIMIZATION RESULTS

### 4.1. Transient Dynamics Analysis under Multi-Working Conditions

In this paper, the full method of FE is used for the TCDDS and TSSS. Based on the deformation energy method, the energy loss ratios of the TCDDS are calculated to be 0.1545 and the energy loss ratios of the TSSS is 0.2914, which shows the vibration-reducing performance of TSSS is better than that of TCDDS.

Figure 7 shows the displacement curves of the damping layers of the TCDDS and TSSS with time. The displacement am-

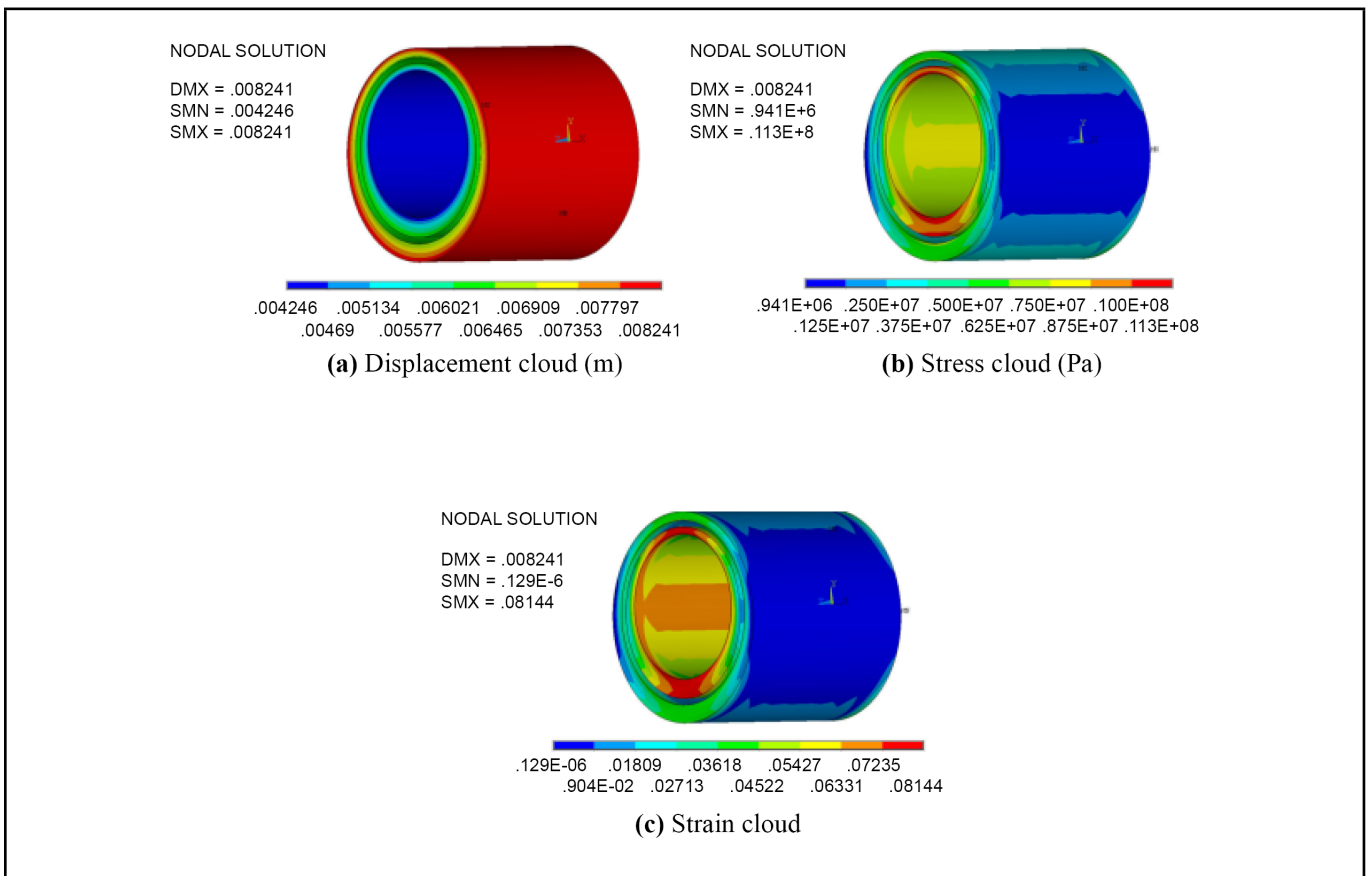


Figure 8. Maximum displacement, stress and strain of “double damping layer” of the original structure.

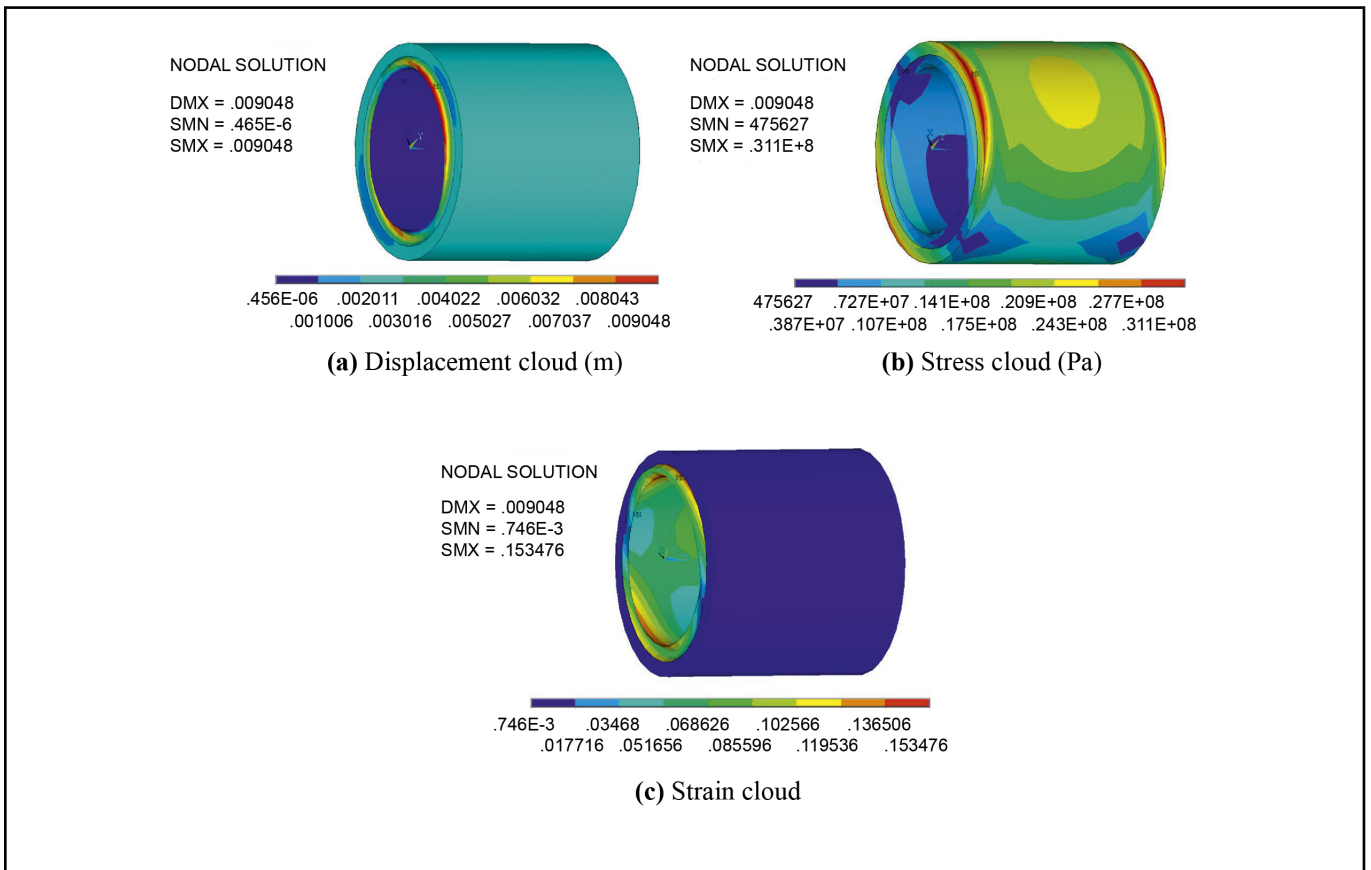
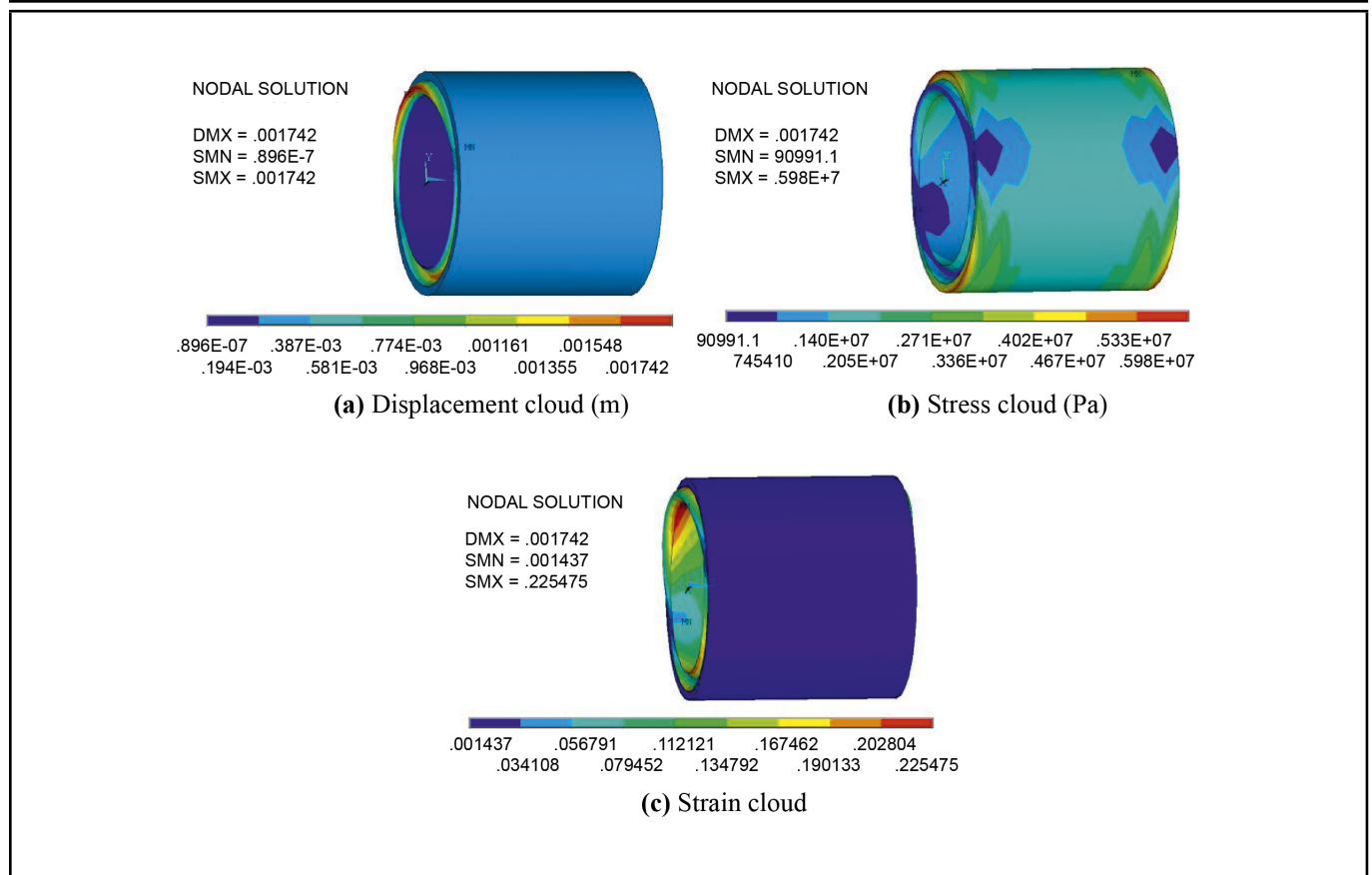


Figure 9. Maximum displacement, stress, strain cloud of “damping layer + stand-off-layer” before optimization.



**Figure 10.** Maximum displacement, stress, strain cloud of damping layer and stand-off-layer after optimization.

plitude of the damping layers of the two structures gradually increases with time, and each curve almost maintains a linear change, which is related to the constitutive model of the rubber material of the damping layer selected in ANSYS and the damping coefficient value set in ANSYS. In the Fig. 7, the displacement amplitude of the damping layer of the TSSS increases slowly and uniformly with time, and the dynamic amplitude response is stable. While the displacement response of the damping layer of the TCDDS increases rapidly and shows a steep trend. The maximum displacement amplitude of the first damping layer (Five-layer(2)) is 6 times that of TSSS, and the maximum displacement amplitude of the second damping layer(Five-layer(4)) is 12 times that of TSSS. In conclusion, the energy dissipation effect of the TSSS proposed in this paper is more obvious than that of the TCDDS.

In addition, the maximum displacement, stress and strain of “double damping layer” and “stand-off-layer+damping layer” can be obtained from the post-processing of transient dynamic analysis, respectively.<sup>26</sup> It can be seen from Fig. 8 that the energy consumption of the TCDDS is mainly caused by the transverse deformation of the “double damping layer”. At the same time, it could be known that the stress concentration of this kind of structure is obvious. It can be seen from Fig. 9 that the energy consumption of the TSSS is enhanced by increasing the shear deformation of “stand-off-layer + damping layer”, and the maximum displacement response is located at the end of damping layer. Furthermore, the maximum stress of “damping layer + stand-off-layer” is located outside the end of stand-off-layer, which is  $3.11 \times 10^7$  Pa, which has exceeded the allowable stress value  $G_{max}$  of damping mate-

rial  $G_{max}$  ( $G_{max} \leq 8.3 \times 10^6$ Pa);<sup>16</sup> The maximum strain of “damping layer + stand-off-layer” is smaller, which is located near the end of damping layer, and is 15.35%. Therefore, the parameters of the structure need to be improved.

Figure 10 shows the dynamic response of the stand-off-layer and damping layer of the optimized structure, Table 3 shows the vibration characteristic parameter values before and after the optimization of the TSSS. It can be seen from Fig. 10 and Table 3 that the maximum displacement and maximum stress of the damping layer and stand-off-layer of the optimized structure are greatly reduced, and the maximum stress meets the allowable stress of damping material  $G_{max}$  ( $G_{max} \leq 8.3 \times 10^6$ Pa); The maximum strain of damping layer and stand-off layer of the optimized structure increases from 15.35% to 22.55%; The energy loss ratio increased from 0.2914 to 0.5418. In conclusion, the results show that the energy dissipation effect of the TSSS can be more significant and the design parameters can be more reasonable by using this optimization design.

#### 4.2. Verification by Modal Analysis

Using the modal strain energy method,<sup>23</sup> through modal analysis, the natural frequencies of the first six modes and loss factors of the structure before and after optimization are compared.

It can be seen from Table 4 that with the gradual increase of modal order, the natural frequency of the TSSS also increases gradually, and at the same time the natural frequency of the third-order to the fourth-order modes of the structure increases greatly, also the modal loss factor increases first and

**Table 3.** Comparison of results before and after optimization under multiple working conditions.

Category	Before optimization	After optimization	Difference	Percentage
Maximum displacement (m)	0.009048	0.001742	-0.007306	-80.747%
Maximum stress (Pa)	$0.311 \times 10^8$	$0.598 \times 10^7$	$-0.2512 \times 10^8$	-80.772%
Maximum strain	0.153476	0.225475	+0.071999	+46.912%
Energy loss ratio $\eta$	0.2914	0.5418	+0.2504	+85.930%

**Table 4.** Modal natural frequency and loss factor before and after optimization.

Modal Order	Before Optimization		After Optimization	
	Natural frequency (Hz)	Loss factor	Natural frequency (Hz)	Loss factor
1	180.69	0.29	203.12	0.34
2	232.34	0.14	261.22	0.20
3	562.55	0.42	583.42	0.50
4	1243.4	0.25	1118.5	0.32
5	1607.6	0.19	1556.3	0.23
6	1626.3	0.18	1601.2	0.20

decreases. The natural frequencies of the first three modes of the structure before optimization are slightly lower than those after optimization, and the difference is about 20Hz, while the natural frequencies of the last three modes are slightly higher than those after optimization. Compared with the loss factor of the structure before optimization, the loss factors of the first six modes of the structure after optimization increase greatly, the average value added is about 0.053. In summary, the resonance frequency of the optimized structure in the low frequency band is increased slightly, the resonance frequency in the high frequency band decreased. At the same time, the modal loss factor and vibration-reducing performance of the structure is significantly enhanced.

## 5. CONCLUSION

Aiming at the problem of low vibration reduction efficiency of the vibration damping structure of the driving sprocket of tracked construction vehicle under multiple working conditions, this paper based on niche technique and adaptive idea, the structural parameters and geometric parameters of tubular transition damping structure are optimized by using ANSYS and MATLAB, to improve the vibration-reducing performance of the structure.

The specific conclusions are as follows:

1. The main failure mode of the damping layer in the TCDDS is stress failure, and the stress is concentrated near the end of the damping layer.
2. The energy consumption of TCDDS is mainly caused by the transverse deformation of the “double damping layer”, while the energy consumption of the TSSS is enhanced by increasing the torsional shear deformation of the “stand-off-layer + damping layer”. The energy loss ratios of the TCDDS and the TSSS are 0.1545 and 0.2914 respectively. In summary, the energy consumption effect of the latter is more obvious than that of the former.
3. After optimization, the maximum displacement and maximum stress of “damping layer + transition layer” are greatly reduced, the maximum strain increases from 15.35% to 22.55%, the energy loss ratio increases from 0.2914 to 0.5418, and the growth rate is 85.93%. The vibration damping effect is obviously improved.

## 6. ACKNOWLEDGEMENTS

Research Funded through Natural Science Foundation of Shanxi Province (Project No. 201901D111246), Shanxi Provincial Basic Research Program (Project No. 20210302123275) and Doctoral Scientific Research Foundation of Taiyuan University of Science and Technology (Project No. 20192021).

## REFERENCES

- 1 Sun, D. G., Zhu, W. N., and Gong, K. J. Study on damping and vibration reduction of large crawler bulldozer, *Journal of mechanical engineering*, **34**(1), 27–33, (1998). <https://doi.org/10.3321/j.issn:0577-6686.1998.01.005>
- 2 Sun, D. G., Zhu, W. N., Ma, W. D., et al. Development of rubber buffer device for large and super large crawler bulldozers, *Mechanical design*, **15**(4), 29–31, (1998). <https://doi.org/10.3969/j.issn.1001-2354.1998.04.011>
- 3 Yellin, J. M., Shen, I. Y., and Reinhall, P. G. Experimental and finite element analysis of stand-off layer damping treatments for beams, *Smart Structures and Materials 2005: Damping and Isolation*, **5760**, 89–99, (2005). <https://doi.org/10.1117/12.599879>
- 4 Rogers L. C., and Parin, M. Experimental results for stand-off passive vibration damping treatment, *Smart Structures and Materials 1995: Passive Damping*, **2445**, 374–383, (1995). <https://doi.org/10.1117/12.208903>
- 5 W. G. Z., Y. F. L., S. D. Li, et al. Topology Optimization of Passive Constrained Layer Damping with Partial Coverage on Plate, *Shock and Vibration*, **20**(2), 199–211, (2013). <https://doi.org/10.1155/2013/360327>
- 6 Zhang, F., Guo, M., Xu, K., et al. Multilayered damping composites with damping layer/constraining layer prepared by a novel method, *Composites Science and Technology*, **101**, 167–172, (2014). <https://doi.org/10.1016/j.compscitech.2014.06.021>
- 7 Yan, B. J., Zhao, Z. D., Lang, B. X., et al. Damping characteristic analysis and application of a tubular stand-off-layer

- sandwiched structure, *Noise Control Engineering Journal*, **65**(6), 522–530, (2017).<https://doi.org/10.3397/1/376566>
- <sup>8</sup> Zhang, W. J., Sun, D. G., Li, Z. L., et al. Analysis of damping characteristics of tubular stand-off-layer sandwiched structure, *Journal of Applied Basic Science and Engineering*, **28**(02), 460–474, (2020).<https://doi.org/10.16058/j.issn.1005-0930.20209.02.019>
- <sup>9</sup> Kingan, M. J., Yang, Y., and Mace, B. R. Sound transmission through cylindrical structures using a wave and finite element method, *Wave Motion*, **87**, 58–74, (2019).<https://doi.org/10.1016/j.wavemoti.2018.07.009>
- <sup>10</sup> Goldberg, D. E., and Richardson. J. Genetic algorithms with sharing for multimodal function optimization, *Genetic algorithms and their applications: Proceedings of the Second International Conference on Genetic Algorithms*, Vol. 4149, Hillsdale, NJ: Lawrence Erlbaum, (1987).
- <sup>11</sup> Ji, Q. L., Qi, W. M., Cai, W. Y., et al. Study of improved hierarchy genetic algorithm based on adaptive niches, *International Conference on Intelligent Computing*, 1014–1022, (2005). <https://doi.org/10.1109/icmlc.2005.1527760>
- <sup>12</sup> Shi, H.R. Vibration analysis and optimization of locally viscoelastic constrained damping beam, Dalian University of technology, Dalian, China, (2008).
- <sup>13</sup> Kumar, K. K., Pabboju, S. An efficient adaptive genetic algorithm technique to improve the neural network performance with aid of adaptive GA operators, *International Journal of Networking & Virtual Organisations*, **20**(2), 127–142, (2019).<https://doi.org/10.1504/ijnvo.2019.10007705>
- <sup>14</sup> Chen, X., Zhang, B., and Gao, D. Algorithm Based on Improved Genetic Algorithm for Job Shop Scheduling Problem, *2019 IEEE International Conference on Mechatronics and Automation (ICMA)*, 951–956, (2019).<https://doi.org/10.1109/icma.2019.8816334>
- <sup>15</sup> Bai, J., Tian, M., and Li, J. An Elite Adaptive Niche Evolutionary Algorithm for Duty Clustering Problem in SoWSN, *Journal of Physics: Conference Series*, IOP Publishing, **1769**(1), 012067, (2021).<https://doi.org/10.1088/1742-6596/1769/1/012067>
- <sup>16</sup> Ni, J. T., Sun, D. G., and Yi, Z. C. Structural parameter optimization of viscoelastic suspension damping buffer, *Construction machinery*, **5**, 76–79, (2010).<https://doi.org/10.3969/j.issn.1001-554X.2010.03.018>
- <sup>17</sup> Sun, D.G., and Zhu, W.N. Series test of rubber shock absorber, *Construction machinery*, **3**, 11–14, (1997).
- <sup>18</sup> JIS K6385-1977. Testing methods for rubber vibration isolators, Japanese Standards Association, (1989).
- <sup>19</sup> Ding, X., and Gao, S. Research on text feature selection based on improved invasive weed algorithm, *Electronic design engineering*, **25**(04), 22–26, (2017).<https://doi.org/10.14022/j.cnki.dzsjgc.2017.04.006>
- <sup>20</sup> Qiu, S., and Zhou, J. Y. Collaborative optimization design and application based on MATLAB and ANSYS, *Mechanical design*, **35**(09), 72–76, (2018).<https://doi.org/10.13841/j.cnki.jxsj.2018.09.012>
- <sup>21</sup> Wang, J., Sun, D. G., Liu, S. Z., et al. Damping characteristics of rubber damper considering thermal mechanical coupling, *Vibration: Test and diagnosis*, **38**(04), 859–865+880, (2018). <https://doi.org/10.16450/j.cnki.issn.1004-6801.2018.04.030>
- <sup>22</sup> Madenci, E., and Guven, I. The Finite Element Method and Applications in Engineering Using ANSYS, Springer, (2015). [https://doi.org/10.1007/978-1-4899-7550-8\\_12](https://doi.org/10.1007/978-1-4899-7550-8_12)
- <sup>23</sup> Dai, D.P. Damping and noise reduction technology, Xi'an Jiaotong University Press, Xian, (1986).
- <sup>24</sup> Sun, B., Sun, D. G., Li, Z.L., et al. Modified modal strain energy method for modal loss factor analysis of viscoelastic structures, *Acta Ordnance Engineering Sinica*, **37**(01), 155–164, (2016). <https://doi.org/10.3969/j.issn.1000-1093.2016.01.023>
- <sup>25</sup> Zhang, S.H., Chen, H.L., and Liang, T.X. Numerical simulation of damping properties of fiber reinforced resin matrix composites, *Journal of aeronautical materials*, **24**(3), 10–14, (2004). <https://doi.org/10.3969/j.issn.1005-5053.2004.03.003>
- <sup>26</sup> Wang, A.Q., and Zhang, L. Transient dynamic response analysis of horizontal seismic action of middle hole string dome structure, *Steel structure*, **33**(06), 12–16, (2018).<https://doi.org/10.13206/j.gjg.201806003>

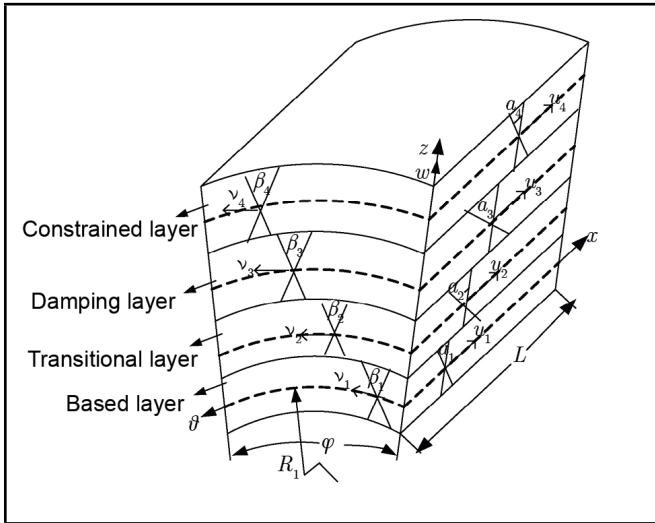
## APPENDIX A

Figure A1 shows a micro element structure of tubular stand-off sandwiched structure in cylindrical coordinates  $(x, \theta, x)$ . According to the shear deformation theory and the motion constraints of each node in each direction, the total displacement at any point in a layer can be generalized as:

$$\begin{aligned} W(x, \theta, z) &= w(x, \theta); \\ V(x, \theta, z) &= v(x, \theta) + h\beta(x, \theta); \\ U(x, \theta, z) &= u(x, \theta) + h\alpha(x, \theta); \end{aligned} \quad (13)$$

where  $u$ ,  $v$ , and  $w$  are the displacements in the axial direction, transverse direction, and radial direction, respectively.  $h$  is the height of the point along the  $z$  direction from the mid-surface of the layer.

Based on the generalized Hooke's law, the stress-strain constitutive relationship of a layer of the tubular stand-off-layer



Note: where  $x$  represents axial direction;  $\theta$  represents peripheral direction;  $z$  represents radial direction;  $(W_i, v_i, u_i)(i = 1, 2, 3, 4)$  are associated displacements of mid-surface for each layer;  $\alpha_i$  and  $\beta_i(i = 1, 2, 3, 4)$  are respectively shear angles for axial and peripheral directions;  $R_i(i = 1, 2, 3, 4)$  is radius of each layer;  $\psi$  is peripheral dimensions;  $L$  is axial dimensions.

Figure A1. Micro-unit of tubular stand-off-layer sandwiched structure.

sandwiched structure can be expressed as:

$$\begin{aligned} \sigma_{xx} &= 2G_i\epsilon_{xx} + \lambda_i\epsilon, \quad \tau_{x\theta} = G_i\gamma_{x\theta}; \\ \sigma_{\theta\theta} &= 2G_i\epsilon_{\theta\theta} + \lambda_i\epsilon, \quad \tau_{\theta z} = G_i\gamma_{\theta z}; \\ \sigma_{zz} &= 2G_i\epsilon_{zz} + \lambda_i\epsilon, \quad \tau_{xz} = G_i\gamma_{xz}; \end{aligned} \tag{14}$$

where  $\epsilon$  is the volumetric strain,  $\epsilon_{xx}, \epsilon_{\theta\theta}, \epsilon_{zz}$  is normal strain,  $\gamma_{x\theta}, \gamma_{\theta z}, \gamma_{xz}$  is the shear strain.  $\lambda_i$  is the Lamé coefficient,  $\lambda_i = \frac{\nu_i E_i}{(1+\nu_i)(1-2\nu_i)}$ ,  $G_i$  is the shear modulus of a layer of material,  $G_i = \frac{E_i}{2(1+\nu_i)}$ ,  $E_i$  and  $\nu_i$  is the elastic modulus and Poisson's ratio of a layer of material respectively,  $i = 1, 2, 3, 4$  corresponding to base layer, stand-off layer, damping layer and constraint layer, as shown in Fig. A1. In addition, it is assumed that the layers do not compress, so  $\partial w / \partial z = 0$  for all layers of the treatment. At the same time, The transverse normal stress  $\sigma_{zz}$  in the  $z$ -direction is assumed to be zero.

The tubular stand-off-layer sandwiched structure belongs to a type of thick cylindrical shell, so the corresponding strain displacement equation of each layer is:

$$\begin{aligned} \epsilon_{xx} &= \frac{\partial u}{\partial x} + z \frac{\partial \alpha}{\partial x}; \\ \epsilon_{\theta\theta} &= \frac{1}{R} \frac{\partial v}{\partial \theta} + \frac{w}{R} + \frac{z}{R} \frac{\partial \beta}{\partial \theta}; \\ \epsilon_{zz} &= 0; \\ \gamma_{x\theta} &= \frac{\partial v}{\partial x} + z \frac{\partial \beta}{\partial x} + \frac{1}{R} \frac{\partial u}{\partial \theta} + \frac{z}{R} \frac{\partial \alpha}{\partial \theta}; \\ \gamma_{\theta z} &= \frac{1}{R} \frac{\partial w}{\partial \theta} - \frac{v}{R} + \beta; \\ \gamma_{xz} &= \frac{\partial w}{\partial x}. \end{aligned} \tag{15}$$

damping layer is:

$$\begin{aligned} U_{xx}^3 &= \frac{1}{2} \int_0^L \int_0^\theta \int_{-H_3/2}^{H_3/2} \sigma_{xx}\epsilon_{xx}(R_3 + z) dx d\theta dz; \\ U_{\theta\theta}^3 &= \frac{1}{2} \int_0^L \int_0^\theta \int_{-H_3/2}^{H_3/2} \sigma_{\theta\theta}\epsilon_{\theta\theta}(R_3 + z) dx d\theta dz; \\ U_{zz}^3 &= 0; \\ U_{xz}^3 &= \frac{1}{2} \int_0^L \int_0^\theta \int_{-H_3/2}^{H_3/2} \tau_{xz}\gamma_{xz}(R_3 + z) dx d\theta dz; \\ U_{\theta z}^3 &= \frac{1}{2} \int_0^L \int_0^\theta \int_{-H_3/2}^{H_3/2} \tau_{\theta z}\gamma_{\theta z}(R_3 + z) dx d\theta dz; \\ U_{x\theta}^3 &= \frac{1}{2} \int_0^L \int_0^\theta \int_{-H_3/2}^{H_3/2} \tau_{x\theta}\gamma_{x\theta}(R_3 + z) dx d\theta dz; \\ U^3 &= U_{xx}^3 + U_{\theta\theta}^3 + U_{zz}^3 + U_{xz}^3 + U_{\theta z}^3 + U_{x\theta}^3; \\ U^3 &= \xi\pi G \int_0^L \int_0^\theta \int_{-H_3/2}^{H_3/2} (\gamma_{x\theta}^2 + \gamma_{\theta z}^2 + \gamma_{xz}^2) \cdot \\ & (R_3 + z) dx d\theta dz; \\ U^3 + U^2, U^3 &= U^2; \end{aligned} \tag{16}$$

where  $U_{xx}^3$  and  $U_{\theta\theta}^3$  are the strain energy of the damping layer due to the combined bending and stretching in the  $x$  and  $\theta$  directions, respectively;  $U_{xz}^3, U_{\theta z}^3, U_{x\theta}^3$  are the strain energy of the damping layer due to the transverse shear strain;  $U^2$  and  $U^3$  are the total elastic deformation energy of the stand-off layer and damping layer;  $U^2$  and  $U^3$  is the shear loss energy of the stand-off layer and damping layer;  $H_3$  is the thickness of the damping layer,  $R_3$  is the radius of the damping layer,  $L$  is the length of the micro element in the  $x$ -direction,  $\xi$  is material loss factor of damping layer, and  $\psi$  is the angular dimension of the element in the circumferential direction.

Similarly, for the base layer, stand-off layer and constraint layer in the micro element structure in Figure 11. Namely, the elastic strain energy of Eq. 8 is obtained by solving. the expressions of elastic strain energy and shear loss energy of each layer are

$$\begin{aligned} U_{xx}^i &= \frac{1}{2} \int_0^L \int_0^\theta \int_{-H_i/2}^{H_i/2} \sigma_{xx}\epsilon_{xx}(R_i + z) dx d\theta dz; \\ U_{\theta\theta}^i &= \frac{1}{2} \int_0^L \int_0^\theta \int_{-H_i/2}^{H_i/2} \sigma_{\theta\theta}\epsilon_{\theta\theta}(R_i + z) dx d\theta dz; \\ U_{x\theta}^i &= \frac{1}{2} \int_0^L \int_0^\theta \int_{-H_i/2}^{H_i/2} \tau_{x\theta}\gamma_{x\theta}(R_i + z) dx d\theta dz; \\ U_1 &= U_4 = U_{xx}^i + U_{\theta\theta}^i; \\ U_1 &= U_4 = U_{x\theta}^i; \end{aligned} \tag{17}$$

where  $U_{xx}^i$  and  $U_{\theta\theta}^i$  is the elastic strain energy in the axial direction and the circumferential direction, and  $U_{x\theta}^i$  is the shear loss energy due to in-plane shear strain  $\gamma_{x\theta}(i = 1, 4)$ .  $U_1, U_4$  are the elastic strain energy and shear loss energy of base layer and constraint layer respectively.

Therefore, in one vibration period, the strain energy of the